Journal of Magnetic Resonance 205 (2010) 269–275

Contents lists available at ScienceDirect

Journal of Magnetic Resonance

journal homepage: www.elsevier.com/locate/jmr

^{1}H homonuclear dipolar decoupling using rotor-synchronised pulse sequences: Towards pure absorption phase spectra

Subhradip Paul [a], Rajendra Singh Thakur [a], M.H. Levitt [b], P.K. Madhu [a,*]

[a] Department of Chemical Sciences, Tata Institute of Fundamental Research, Homi Bhabha Road, Colaba, Mumbai 400 005, India
[b] Department of Chemistry, University of Southampton, SO17 1BJ, UK

ARTICLE INFO

Article history:
Received 20 March 2010
Revised 11 May 2010
Available online 19 May 2010

Keywords:
Solid-state NMR
Homonuclear dipolar decoupling
Symmetry-based pulse sequences
RN_n^ν
*w*PMLG
Pure absorption

ABSTRACT

We demonstrate a pulse sequence using symmetry-based rotor-synchronised RN_n^ν sequences for homonuclear dipolar decoupling that achieves pure absorption phase high-resolution ^{1}H spectra in solid-state NMR. This sequence is compared with the phase-modulated Lee-Goldburg scheme. Experimental results are shown for samples of glycine and L-histidine·HCl·H_2O for magic-angle-spinning frequencies in the range of 14–30 kHz and at two different magnetic fields.

1. Introduction

Solid-state nuclear magnetic resonance (NMR) spectroscopy of abundant nuclei, such as ^{1}H, is rendered difficult by the presence of strong homonuclear dipolar couplings. The ^{1}H solid-state NMR spectra of rigid samples are normally broad, even under magic-angle-spinning (MAS), which obscures the chemical shift information. An effective way to enhance the resolution is to average out the strong homonuclear dipolar couplings by applying radio-frequency pulses along with MAS, a technique referred to as combined rotation and multiple-pulse spectroscopy (CRAMPS) [1–3]. Several CRAMPS techniques have been introduced including phase-modulated Lee-Goldburg (PMLG) [4–6] and decoupling under mind boggling optimisation (DUMBO) [7,8]. These schemes have been applied in single-, double- and triple-quantum ^{1}H spectroscopy [8,9]. Developments in this field have been reviewed by Vinogradov et al. [10], Brown [11], and Madhu [12], and practical aspects regarding implementation of these sequences have been summarised by Coelho et al. [13].

Efforts to improve the performance of the PMLG scheme have led to better understanding of the role of RF imperfections and the significance of effective *z*-rotations [14–16]. The introduction of windowed acquisition has helped the acquisition of high-resolution ^{1}H spectra in both one-dimensional (1D) and two-dimensional (2D) protocols [17]. The introduction of supercycled schemes has enabled these methods to be applied at high MAS frequencies up to 65 kHz [18,19]. Recently we have introduced new supercycling schemes for *w*PMLG and *w*DUMBO which resulted in increased robustness with respect to the MAS frequency [20].

At certain ratios of the pulse sequence cycle frequency (ν_c) and the MAS frequency (ν_r), resonant interference occurs which leads to line broadening and the appearance of extra lines in the spectrum [10]. Another disadvantage of *w*PMLG and *w*DUMBO sequences is the requirement of high RF fields at higher MAS frequencies which restricts the application of these sequences to low or moderate spinning frequencies [19]. A different approach is to use rotor-synchronised sequences as demonstrated by Demco, Hafner, Spiess, and the group of Levitt [21–23]. Two sets of experiments have been developed which are based on symmetry principles and rotor synchronisation. One method utilises symmetry-based pulse sequences of the *R* type consisting of composite 180° pulses [23,24] and the other utilises smooth amplitude modulation [25,26].

We recently presented preliminary results which demonstrate the potential of these symmetry sequences in the field of homonuclear dipolar decoupling [24]. However, the implementation chosen for that initial demonstration did not achieve pure-absorption line shapes in the 2D spectrum, and generated quadrature image peaks. In this work we use a modified pulse sequence in order to achieve 2D spectra in pure absorption phase and without image peaks. We additionally compare $w\text{PMLG}_{mm}^{x\bar{x}}$ and RN_n^ν sequences for homonuclear decoupling with spectra from two magnetic fields at proton Larmor frequencies of 500 and 700 MHz. We

* Corresponding author. Fax: +91 22 2280 4610.
E-mail address: madhu@tifr.res.in (P.K. Madhu).

1090-7807/$ - see front matter © 2010 Elsevier Inc. All rights reserved.
doi:10.1016/j.jmr.2010.05.009

also demonstrate the potential of the symmetry-based pulse sequences in hetero-correlation spectroscopy.

2. Experimental

The *w*PMLG and RN_n^ν experiments were carried out on Bruker AVI 500 MHz and AVIII 700 MHz spectrometers. The exact details are listed in the figure captions. Commercially available glycine, L-histidine·HCl·H_2O, and U–^{13}C–L-histidine·HCl·H_2O samples were used without any purification or recrystallisation. A sample of commercially available adamantane was used for the calibration of the proton nutation frequency.

3. Results and discussions

The RN_n^ν symmetry sequences of the form $[R_\phi R'_{-\phi}]^{N/2}$ consist of $\frac{N}{2}$ pairs of the pulse block $[R_\phi R'_{-\phi}]$ spanning n rotor periods, where ϕ is the overall phase shift given by $\phi = \frac{\pi}{N}\nu$, where $\nu$is the spin winding number [27]. The element R_ϕ is derived from the basic element R^0 by an overall phase shift of ϕ. The element $R'_{-\phi}$ is derived from R_ϕ by changing the sign of all phases. The basic element R^0 rotates resonant spins by an odd multiple of π about the x-axis. Typically, the basic element R^0 is a single or composite 180° pulse [27].

The synchronisation of the space and spin trajectories generates an average Hamiltonian for which certain desired combinations of $\{l, m, \lambda, \mu\}$ are allowed and the other combinations are suppressed. The spin interactions are classified here according to the quantum numbers $\{l, m, \lambda, \mu\}$ where $\{l, m\}$ indicates the transformation properties of these interactions with respect to the spatial rotation of the molecular framework and $\{\lambda, \mu\}$ indicates the transformation properties of these interactions with respect to the rotation of the nuclear spins induced by RF irradiation. For high-resolution ^{1}H spectroscopy the isotropic chemical shift interaction $l = 0$ and $\lambda = 1$ should be symmetry-allowed whilst chemical shift anisotropy terms ($l = 2$, $\lambda = 1$), homonuclear dipolar couplings ($l = 2$, $\lambda = 2$), and heteronuclear dipolar couplings ($l = 0$, $\lambda = 2$) should all be symmetry-forbidden [27]. RN_n^ν sequences having a spin winding number set as $N/2$ are suitable for use as homonuclear decoupling sequences since they allow terms of the form $\{0, 0, 1, \mu\}$ whilst terms of the form $\{2, m, \lambda, \mu\}$ are symmetry-forbidden. A list of suitable RN_n^ν sequences having $N \leqslant 20$, $n \leqslant 5$ and $\nu \leqslant 10$ is provided in Table 1. All of these symmetries allow isotropic chemical shifts, homonuclear, and heteronuclear J-couplings but suppress CSA, homonuclear, and heteronuclear dipolar couplings. For all RN_n^ν sequences of this type, the effective rotation axis of the chemical shift Hamiltonian is the x-axis. Detailed study of these symmetry sequences is given in Ref. [27].

For better performance with respect to off-resonance and in order to improve local averaging of the homonuclear dipolar interactions the RN_n^ν sequences used here are based on the composite pulse elements. Here, element $R^0 = 90_{-45}90_{45}90_{-45}$. Although the RN_n^ν symmetry ensures that the first-order average Hamiltonian has an appropriate form, the performance of a particular implementation depends on the magnitude and form of the higher-order terms. Higher-order terms involving homonuclear dipolar couplings may be minimised by ensuring that the first-order average Hamiltonian, taken over a single R-element, is as small as possible. This implies that the R-element itself should implement good local averaging of the homonuclear dipolar interactions. For this reason we use the basic element $R^0 = 90_{-45}90_{45}90_{-45}$ which provides a 180° rotation around the x-axis, with a vanishing local average of homonuclear dipolar interactions in the quasi static limit (composite pulse duration short compared to a rotor period) [23,27]. The explicit RN_n^ν sequence is therefore given by (see Table 2)

Table 1
RN_n^ν symmetries for the observation of isotropic chemical shifts, homonuclear, and heteronuclear J couplings under MAS. All the mentioned RN_n^ν sequences select isotropic chemical-shift terms $(l, m, \lambda, \mu) = (0, 0, 1, \pm1)$. All the CSA and homonuclear DD coupling terms are suppressed. All inequivalent symmetries in the range of $N \leqslant 20$, $n \leqslant 5$ and $\nu \leqslant 10$ are shown.

$n = 1$	$R6_1^3$ $R8_1^4$ $R10_1^5$ $R12_1^6$ $R14_1^7$ $R16_1^8$ $R18_1^9$ $R20_1^{10}$
$n = 2$	$R6_2^3$ $R10_2^5$ $R14_2^7$ $R18_2^9$
$n = 3$	$R8_3^4$ $R10_3^5$ $R14_3^7$ $R16_3^8$ $R20_3^{10}$
$n = 4$	$R6_4^3$ $R10_4^5$ $R14_4^7$ $R18_4^9$
$n = 5$	$R6_5^3$ $R8_5^4$ $R12_5^6$ $R14_5^7$ $R16_5^8$ $R18_5^9$

Table 2
A table of RN_n^ν sequences used to obtain high-resolution ^{1}H spectra shown in Figs. 3–8. MAS frequency and RF power required are given for various RN_n^ν sequences having the composite pulse scheme of $90^\circ_{45}90^\circ_{135}90^\circ_{45}$ as the basic R-element.

RN_n^ν sequences	MAS rate (ν_r in kHz)	RF power (ν_{nut} as a multiple of ν_r)	RF power needed (ν_{nut} in kHz)
$R10_1^5$	14	$7.5\nu_r$	105.0
$R10_1^5$	15	$7.5\nu_r$	112.5
$R14_2^7$	20	$5.25\nu_r$	105.0
$R8_1^4$	20	$6.0\nu_r$	120.0
$R16_3^8$	30	$4.0\nu_r$	120.0

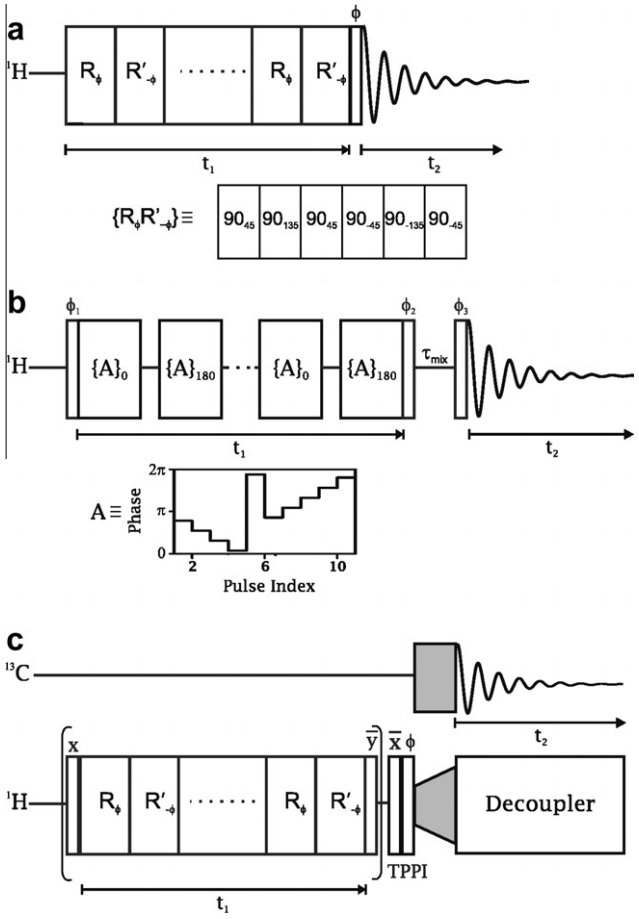

Fig. 1. (a) Pulse sequence employing RN_n^ν scheme to observe ^{1}H chemical shifts that does not lead to pure absorption line shapes the modified form of which is given in Fig. 2. (b) Pulse sequence employing wPMLG$^{\bar{x}\bar{x}}_{mm}$ in the indirect dimension with A depicting the phase profile of a wPMLG block. The 90° pulses are phase cycled as $\phi_1 = [x, y, \bar{x}, \bar{y}]$, $\phi_2 = [\bar{x}, \bar{y}, x, y]$ and $\phi_3 = [x, y, \bar{x}, \bar{y}]$. (c) Pulse sequence used for ^{1}H–^{13}C 2D correlation spectroscopy. Following a t_1 evolution under RN_n^ν sequence the proton magnetisation is transferred to the carbon using RAMP-CP and detected whilst the protons are decoupled using SW$_f$-TPPM [33]. Here $\phi = [x, y, \bar{x}, \bar{y}]$.

$$RN_n^\nu = \{(90_{-45}90_{45}90_{-45})_{90}(90_{45}90_{-45}90_{45})_{-90}\}^{N/2} = \{(90_{45}90_{135}90_{45})(90_{-45}90_{-135}90_{-45})\}^{N/2} \quad (1)$$

where $N/2$ repetitions of the bracketed elements span n rotor periods. The nutation frequency is given by $\nu_{nut} = 0.75\nu_r N/n$ [23]. In practice, the resonance offset of the RF carrier is optimised experimentally for the best resolution, as discussed below.

3.1. R-sequences for high-resolution ^{1}H spectroscopy

In order to obtain high-resolution ^{1}H spectra with RN_n^ν sequences, they need to be implemented in a two-dimensional (2D) way. Homonuclear decoupling is applied during the evolution interval, whilst no decoupling sequence is applied during the signal acquisition. Magic-angle-spinning (MAS) is conducted throughout. The high-resolution ^{1}H spectrum is obtained by taking a positive sum projection on to the indirect frequency axis.

In our previous work [23,24] we employed RN_n^ν sequences in the manner shown in Fig. 1a. The R-sequences rotate the proton z-magnetisation around the x-axis under the scaled chemical shift Hamiltonian. The modulated z-magnetisation is monitored through the amplitude of the signal induced by a 90° read pulse. However, the resulting spectra suffered from phase-twisted line shapes and image peaks.

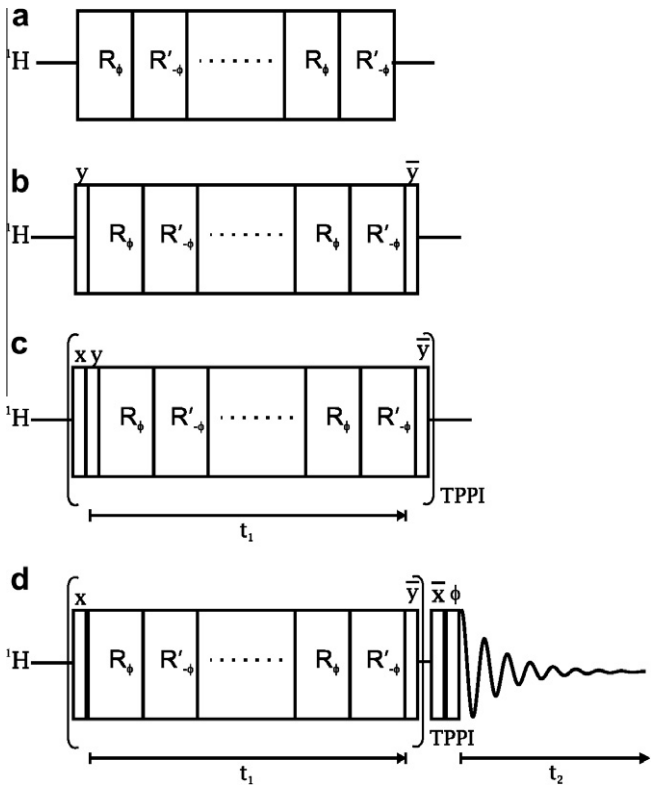

Fig. 2. Step-wise schematic of the modification of the RN_n^ν pulse sequence shown in Fig. 1a to achieve pure phase absorption spectra and to eliminate the image peaks. (a) RN_n^ν block having an effective x-axis of rotation is (b) bracketed by two 90° pulses of phase y and $\bar{y}$ in order to switch the effective axis to z-axis. (c) RN_n^ν block modified for the application of TPPM along with insertion of an initial 90° of phase $x$for excitation of transverse magnetisation. The phase of the entire block is subjected to phase incrementation in synchrony with the incrementation of the evolution interval, t_1 (TPPI). (d) The final form of the pulse sequence. This is constructed from (c) by omitting the redundant second 90°_y pulse and adding two 90° pulses of phases $\bar{x}$ and ϕ respectively before detecting the magnetisation. The penultimate pulse puts the magnetisation to the z-axis which is detected by employing a 90° read pulse, the phase cycling of which is given by $\phi = [x, y, \bar{x}, \bar{y}]$ [28]. The receiver follows the phases of the last pulse. The details of the modification are described in the text.

The performance of the sequence in Fig. 1a is improved by the modifications shown in Fig. 2. First the RN_n^ν sequence, Fig. 2a, is bracketed by two 90° pulses with phase $+y$ and $-y$ as shown in Fig. 2b. This rotates the effective field of the RN_n^ν sequence from the x-axis to the z-axis. After this manipulation, radio-frequency phase shifts, which also act as rotations about the z-axis, commute with the chemical shift evolution and may be used to implement phase shift schemes for pure absorption spectroscopy, as in conventional solution NMR. One possibility is illustrated in Fig. 2c, which shows the modified RN_n^ν sequence incorporated into a typical two-dimensional data acquisition scheme including time-proportional phase-incrementation (TPPI) [29] of single-quantum coherences excited by an initial 90° pulse with phase x. The scheme in Fig. 2d includes two further refinements. First, the second 90° pulse has been removed. This is possible since the initial 90_x pulse is applied to thermal equilibrium magnetisation along the z-axis. The state after this pulse always commutes with the second 90° pulse, which is therefore superfluous. Second, the detected magnetisation is passed through a filter consisting of two further 90° pulses. The penultimate pulse transforms the transverse magnetisation into longitudinal magnetisation, and the last pulse converts this z-magnetisation into observable single-quantum coherences. The phase of the last pulse is varied in a four-step phase cycle in synchrony with the detection phase. This selects NMR signals passing through z-magnetisation at the junction of the last two 90° pulses. This process suppresses any signal components with inappropriate phases. This is the complete modified sequence, Fig. 2d, used here for the acquisition of high-resolution ^{1}H pure absorption phase spectra.

Fig. 3 compares the ^{1}H spectra of glycine obtained using the pulse sequence in Fig. 1a and the pulse sequence in Fig. 2d at

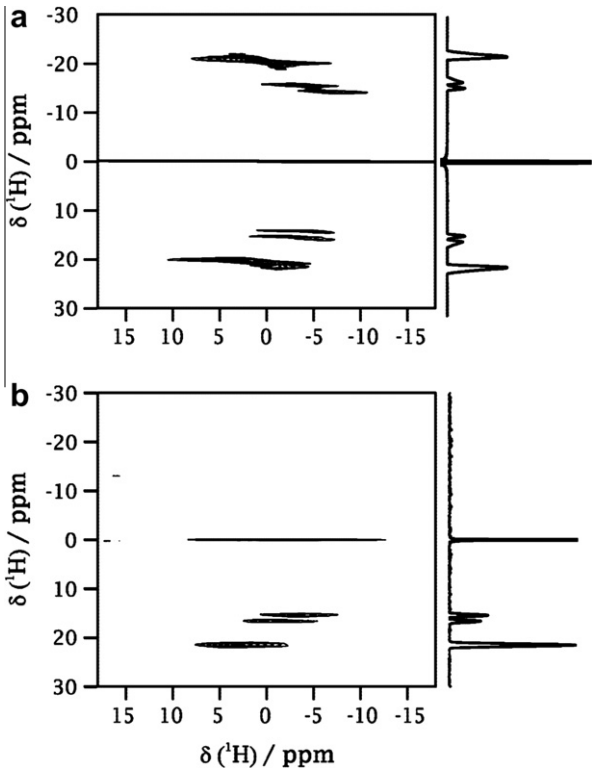

Fig. 3. 2D ^{1}H–^{1}H correlation spectra of glycine obtained using the pulse sequence shown in (a) Fig. 1a and (b) Fig. 2d with $R14_2^7$. The F_1(vertical) proton spectra is the projection of the indirect dimension of the 2D spectra the chemical shifts of which were scaled by a factor of 0.6. The experiments were performed at a spinning frequency of 20 kHz on a Bruker 500 MHz AVI spectrometer using a 2.5 mm double-resonance probe.

20 kHz MAS frequency using $R14_2^7$. The line shapes obtained using the pulse sequence in Fig. 1a display phase distortions and strong image peaks. With the use of the pulse sequence in Fig. 2d image peaks disappear and pure-absorption line shapes are obtained as shown in Fig. 3b. An enhancement in resolution is also obtained which is reflected by the decrease in the linewidth of the NH_3^+ resonance from 0.92 ppm in Fig. 3a to 0.5 ppm in Fig. 3b. In both the cases 1024 points were taken in the indirect dimension with 4 s of recycle delay between each of the four scans per t_1 increment. The carrier frequency was optimised for both cases and was kept −10 kHz from the centre of the proton spectra [30].

Fig. 4 shows the spectra of glycine, left panel, and L-histidine·HCl·H_2O, right panel, obtained at MAS frequencies of 15, 20, and 30 kHz. These spectra are the projections of the indirect dimension of the 2D ^1H–^1H homocorrelation spectra obtained with the pulse sequence in Fig. 2d. The symmetry sequences used in the case of glycine are $R10_1^5$, $R14_2^7$, and $R16_3^8$ whilst in the case of L-histidine·HCl·H_2O they are $R10_1^5$, $R8_1^4$, and $R16_3^8$. The spectra of glycine were referenced by assigning the mid-point of the two methylene proton resonances to be at 3.55 ppm whilst spectra of L-histidine·HCl·H_2O were referenced by assigning the methylene resonance to be at 3.2 ppm. The experimentally obtained scaling factor in all the cases was 0.6. Theoretically the scaling factor is 0.64. The carrier frequency was kept at −10 kHz from the centre of the ^1H spectra.

Fig. 5 shows the projections of the indirect dimension of the 2D ^1H–^1H homocorrelation spectra of glycine at various off-resonance values. These spectra were recorded at 20 kHz of MAS frequency using $R14_2^7$. The spectra indicate that the best decoupling conditions are obtained at high off-resonance values. The best spectra obtained are at +7 kHz and −10 kHz of off-resonance value from the center of the proton spectra taking into account the sign of the precession frequency [30]. No decoupling was observed when the carrier frequency was kept either on the NH_3^+ resonance or on the CH_2 resonance.

In Fig. 6 the scale factor, obtained by measuring the NH_3^+ line position (ΔN) as a function of the RF off-resonance ($\Delta\nu$), is plotted for the sequence $R14_2^7$. A scale factor of 0.6 was obtained which remains constant with respect to the off-resonance values. The

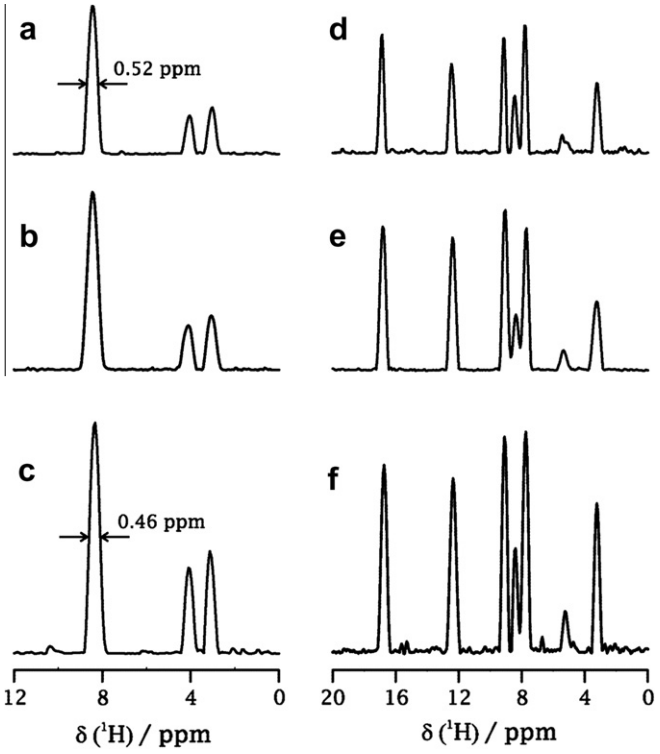

Fig. 4. Projections of the indirect dimension of ^1H–^1H correlation spectra of glycine (left panel) and L-histidine·HCl·H_2O (right panel) obtained using the pulse sequence shown in Fig. 2d. The spectra were recorded at spinning frequencies of (a) 15 kHz using $R10_1^5$, (b) 20 kHz using $R14_2^7$, (c) 30 kHz using $R16_3^8$, (d) 15 kHz using $R10_1^5$, (e) 20 kHz using $R14_2^7$, and (f) 30 kHz using $R16_3^8$. The RF power needed for these sequences are listed in Table 2. The chemical shifts were scaled by a factor of 0.6. The experiments were performed on a Bruker 500 MHz AVI spectrometer using a 2.5 mm double-resonance probe.

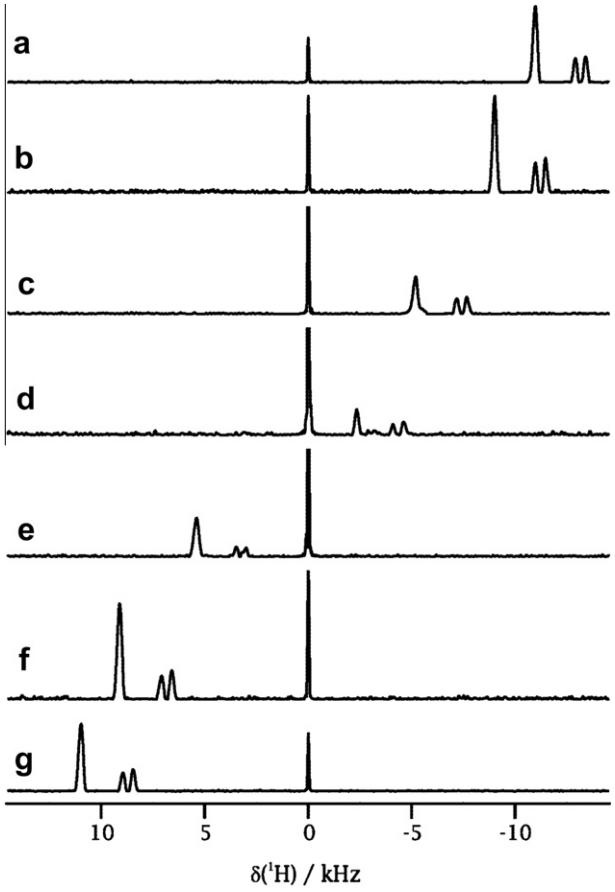

Fig. 5. Projections of the indirect dimension of ^1H–^1H correlation spectra of glycine plotted as a function of off-resonance. The off-resonance values are (a) +9 kHz (b) +7 kHz (c) +3 kHz (d) −1 kHz (e) −5 kHz (f) −10 kHz, and (g) −13 kHz. The spectra were recorded at 20 kHz of spinning frequency using $R8_1^4$ on a Bruker 500 MHz AVI spectrometer using a 2.5 mm double-resonance probe.

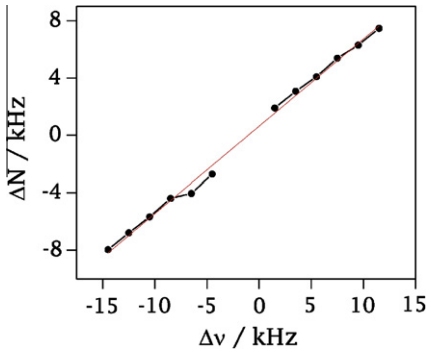

Fig. 6. The off-resonance dependence ($\Delta\nu$) of the NH_3^+ line position (ΔN) of glycine with $R14_2^7$ at 20 kHz of spinning frequency. The experiments were performed on a Bruker 500 MHz AVI spectrometer using a 2.5 mm double-resonance probe. The straight line is the best-fit line with a slope of 0.6 which gives the scale factor of the sequence.

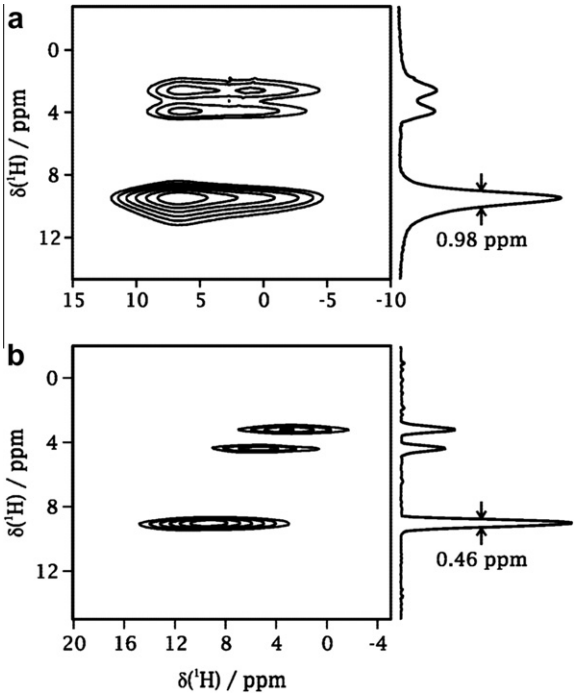

Fig. 7. 2D ^{1}H–^{1}H correlation spectra of glycine obtained using the pulse sequence in (a) Fig. 2d and (b) Fig. 1b. The linewidth of NH_3^+ peak of glycine is indicated on the figure. The experiments were performed at 14 kHz spinning frequency on a Bruker 500 MHz AVI spectrometer using a 4 mm triple-resonance probe.

experimentally obtained line shows a discontinuity as no decoupling was observed when the carrier was kept on resonance. The straight line is the best-fit line with a slope of 0.6 which determines the scale factor $s = \Delta N/\Delta\nu$.

3.2. Comparison of *w*PMLG$^{x\bar{x}}_{mm}$ and RN$^{\nu}_{n}$ schemes of decoupling

Here we compare spectra acquired with RN$^{\nu}_{n}$ and *w*PMLG$^{x\bar{x}}_{mm}$ schemes with both the schemes applied during t_1. The 2D pulse sequence with *w*PMLG$^{x\bar{x}}_{mm}$ is shown in Fig. 1b. For the comparison study, 2D ^{1}H–^{1}H correlation experiments were performed in a similar fashion with *w*PMLG$^{x\bar{x}}_{mm}$ and RN$^{\nu}_{n}$ sequence in the indirect dimension and acquisition under MAS in the direct dimension. These experiments were done on a 4 mm triple-resonance probe at 14 kHz MAS frequency. In both cases, 1024 points were taken in the indirect dimension with 4 s of recycle delay between each of the 4 transients. The carrier was kept on-resonance in case of decoupling under *w*PMLG$^{x\bar{x}}_{mm}$ scheme whilst it was kept at +7 kHz from the center of the ^{1}H spectrum in case of decoupling under RN$^{\nu}_{n}$ scheme. The dwell time in case of decoupling with RN$^{\nu}_{n}$ sequence corresponded to the duration of $[R_\phi R'_{-\phi}]$ which was equal to one 540° pulse. The RN$^{\nu}_{n}$ sequence used in this case was $R10^5_1$ which required a nutation frequency of 105 kHz corresponding to a dwell time of 14.29 μs. The dwell time in case of decoupling under *w*PMLG$^{x\bar{x}}_{mm}$ corresponded to $\tau_c^{x\bar{x}}/2$ which was 20.9 μs. The RF power applied in this case was 97.6 kHz. In spite of having a lower digital resolution, the performance of RN$^{\nu}_{n}$ sequence was better than that of *w*PMLG$^{x\bar{x}}_{mm}$ which is reflected by the linewidth as

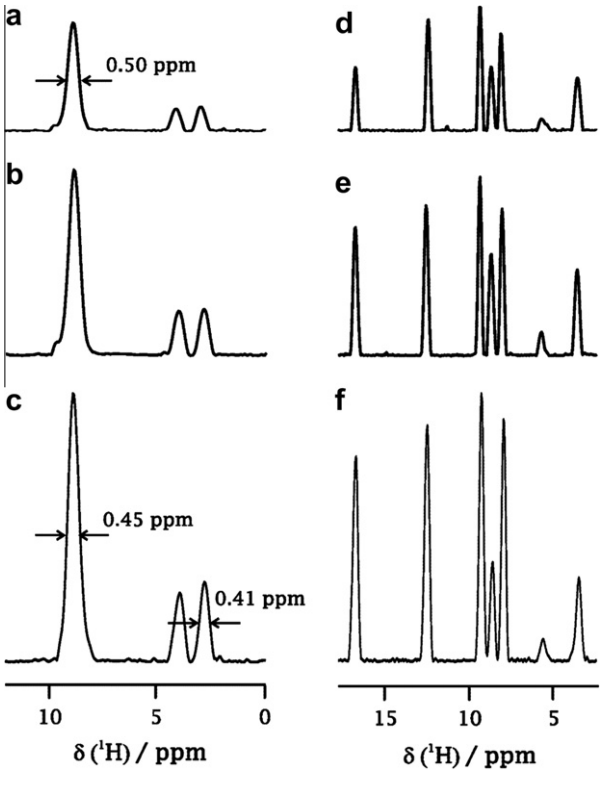

Fig. 8. Projections of the indirect dimension of ^{1}H–^{1}H correlation spectra of glycine (left panel) and L-histidine·HCl·H_2O (right panel) obtained using the RN$^{\nu}_{n}$ schemes shown in Fig. 2d. The spectra were recorded at spinning frequencies and RF nutation frequencies of (a, d) 15 kHz and 112.5 kHz using $R10^5_1$, (b, e) 20 kHz and 120 kHz using $R8^4_1$, and (c, f) 25 kHz and 131.25 kHz using $R14^7_2$. The chemical shifts were scaled by a factor of 0.6. The experiments were performed on a Bruker 700 MHz AVIII spectrometer using a 2.5 mm triple-resonance probe. The offset was placed at −10 kHz from the centre of the spectrum.

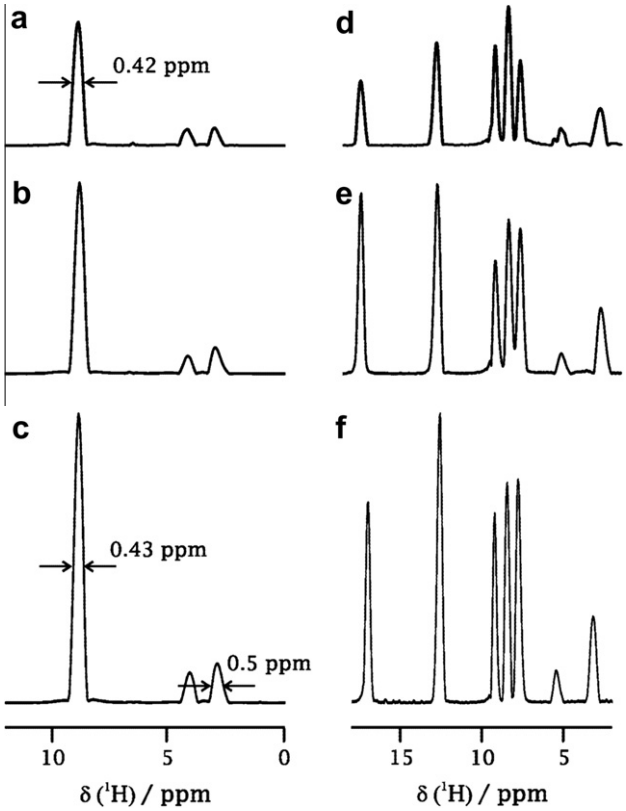

Fig. 9. Projections of the indirect dimension of ^{1}H–^{1}H correlation spectra of glycine (left panel) and L-histidine·HCl·H_2O (right panel) obtained using *w*PMLG$^{x\bar{x}}_{mm}$ scheme shown in Fig. 1b. The spectra were recorded at spinning frequencies and RF nutation frequencies of (a, d) 15 kHz and 102 kHz (b, e) 20 kHz and 135 kHz, and (c, f) 25 kHz and 157 kHz. The chemical shifts were scaled by a factor of 0.45. The experiments were performed on a Bruker 700 MHz AVIII spectrometer using a 2.5 mm triple-resonance probe. The offset was placed at the centre of the spectrum.

indicated on Fig. 7 and also it can be seen from the figure that the CH_2^{α} and CH_2^{β} peak of glycine are completely resolved to the baseline in case of decoupling under symmetry sequences. The scale factor for wPMLG$_{mm}^{x\bar{x}}$ and RN$_n^{\nu}$ sequence was 0.44 and 0.6 respectively.

3.3. wPMLG$_{mm}^{x\bar{x}}$ and RN$_n^{\nu}$ schemes at higher magnetic fields

The results in the previous sections were all obtained at ^{1}H Larmor frequency of 500 MHz. We now investigate the performance of both RN$_n^{\nu}$ and wPMLG$_{mm}^{x\bar{x}}$ schemes at ^{1}H Larmor frequency of 700 MHz.

Fig. 8 shows the RN$_n^{\nu}$ spectra of glycine (left column) and L-histidine·HCl·H_2O (right column) acquired with MAS frequencies of 15, 20, and 25 kHz, using RN$_n^{\nu}$ sequences R10$_1^5$, R8$_1^4$, and R14$_2^7$ and employing RF nutation frequencies of 112.5, 120, and 131.25 kHz from top to bottom rows. Fig. 9 shows the wPMLG$_{mm}^{x\bar{x}}$ spectra of glycine (left column) and L-histidine·HCl·H_2O (right column) acquired with MAS frequencies of 15, 20, and 25 kHz and employing RF nutation frequencies of 102, 135, and 157 kHz from top to bottom rows. The PMLG pulse was of duration 1.55, 1.35, and 0.96 μs for spectra from top to bottom and the window delay was 4.2 μs in all the cases. Selected line widths are indicated in the figure. In both Figs. 8 and 9 the intensities are plotted normalised with respect to the intensity obtained with MAS frequency of 25 kHz. A gain in intensity with increasing MAS frequencies has been reported with the DUMBO decoupling scheme [31].

Comparing Figs. 7 and 9 it is clear that wPMLG$_{mm}^{x\bar{x}}$ performs much better at the higher magnetic field which in our case also has a newer console of Bruker AVIII compared to Bruker AVI for the lower magnetic field. We believe that the improvement in resolution is mainly due to the better pulse profile, lower RF inhomogeneity, and reduced transient effects in the newer console. On the other hand it seems that the RN$_n^{\nu}$ sequences are much more forgiving with respect to the actual RF and probe features as evident from Figs. 4 and 7. There is no resolution advantage with MAS frequency for wPMLG$_{mm}^{x\bar{x}}$ as reported earlier [19], however, there seems to be some improvement of resolution in the case of RN$_n^{\nu}$ sequences. This is evident from the line width of the NH_3^+ resonance at 15 and 25 kHz of MAS frequency. Another noteworthy feature from Figs. 8 and 9 is the lower RF nutation frequency requirement for the RN$_n^{\nu}$ sequences compared with wPMLG$_{mm}^{x\bar{x}}$. This feature might favour the use of RN$_n^{\nu}$ sequences at ultra-high MAS frequencies.

3.4. Two-dimensional ^{13}C-^{1}H hetero-correlation spectroscopy

Fig. 10 shows the potential of R-sequences in hetero-correlation spectroscopy. The experiments were performed on a sample of U–^{13}C–L-histidine·HCl·H_2O at 20 kHz MAS frequency using the pulse sequence shown in Fig. 1c. During the t_1 time domain the proton magnetisation evolved under R8$_1^4$ decoupling. The homonuclear decoupling was carried out with the carrier on the proton kept at −10 kHz from the center of the ^{1}H resonance. The frequency was then switched to on-resonance whilst the magnetisation was along the z-axis after the t_1 evolution for efficient cross polarisation and heteronuclear decoupling. The polarisation was then transferred to the carbons via ramped cross polarisation with a ramped contact pulse on the proton channel to overcome the small mismatch in the Hartmann-Hahn condition [32]. The RF amplitude used on the ^{1}H and ^{13}C were 69 kHz (mid-point of the ramp with a 10% slope) and 49 kHz respectively. 512 points were taken in the t_1 dimension with 4 s of recycle delay between each of the eight scans per t_1 increment. For short CP mixing times only the protons in close proximity were observed. Hence the CH_2^{α}, CH_2^{β}, and the ring protons are only observed. However for long contact times the transfer of polarisation from H_2O, NH, and NH_3^+ protons

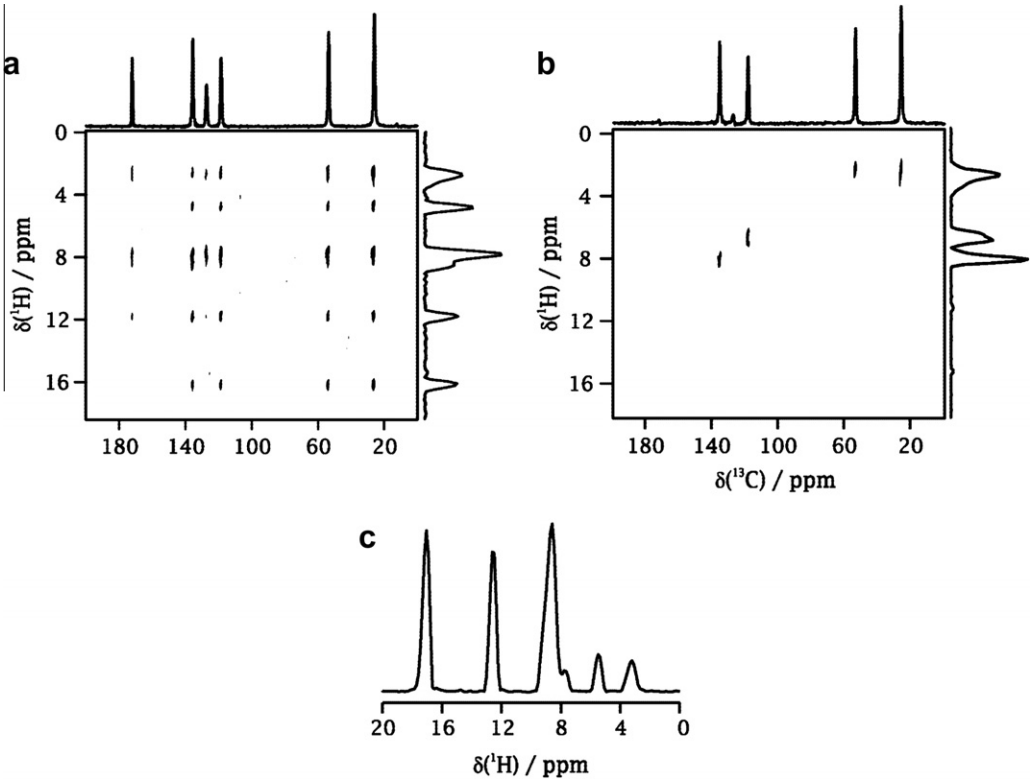

Fig. 10. 2D ^{13}C–^{1}H correlation spectra of U–^{13}C–L-histidine·HCl·H_2O spectra obtained using the pulse sequence shown in Fig. 1c with mixing times of (a) 1 ms and (b) 100 μs. (c) Projection of the indirect dimension of ^{1}H–^{1}H correlation spectrum of U–^{13}C–L-histidine·HCl·H_2O. The experiments were performed at 20 kHz MAS frequency. For homonuclear decoupling $R8_1^4$ was used in the indirect dimension and the carbon magnetisation was detected in the direct dimension while the protons were decoupled using SW$_f$-TPPM [33].

becomes evident in the spectrum. The transfer and build up of polarisation depend on the molecular conformation. The increase in linewidths and absence of the triplet of the ring protons and NH_3^+ as seen in unlabelled L-histidine·HCl·H_2O can be interpreted in terms of the presence of heteronuclear dipolar couplings between ^{13}C and ^1H. To confirm the observation, a 2D homocorrelation ^1H–^1H experiment was performed on the labelled sample with 512 increments in the indirect dimension under the same condition, the result of which is shown in Fig. 10c.

4. Conclusions

The potential of RN_n^ν sequences for high-resolution ^1H spectroscopy in solid-state NMR at high MAS frequencies has been explored in this work. A new pulse sequence protocol allows one to obtain pure-absorption 2D spectra with good resolution and discrimination of the sign of the precession frequency. We have demonstrated ^1H–^1H and ^1H–^{13}C correlation spectroscopy at MAS frequencies of up to 30 kHz. A comparison study between the wPMLG$_{mm}^{x\bar{x}}$ and RN_n^ν sequences shows the following: (a) Resolution with both schemes is comparable with advanced consoles, (b) there is a moderate resolution enhancement with RN_n^ν schemes with increasing MAS frequencies, (c) the RF nutation frequency requirement for RN_n^ν is lower than that for wPMLG$_{mm}^{x\bar{x}}$, and (d) the scale factor for RN_n^ν sequences is higher than that for wPMLG$_{mm}^{x\bar{x}}$.

Acknowledgments

We thank the financial support by the Royal Society (UK) and the British Council of India, the use of National Facility for High-Field NMR, TIFR, for the use of the spectrometers, and M.V. Naik for technical assistance.

References

[1] B.C. Gerstein, C. Clor, R.G. Pembelton, R.C. Wilson, Utility of pulse nuclear magnetic resonance in studying protons in coals, J. Phys. Chem. 81 (1977) 565.
[2] R.E. Taylor, R.G. Pembleton, L.M. Ryan, B.C. Gerstein, High resolution NMR in randomly oriented solids with homonuclear dipolar broadening: combined multiple pulse NMR and magic angle spinning, J. Chem. Phys. 71 (1979) 4541.
[3] B.C. Gerstein, CRAMPS: high resolution NMR of relatively high gamma nuclei, in: R.K. Harris (Ed.), Encyclopedia of Nuclear Magnetic Resonance, John Wiley, 2009.
[4] E. Vinogradov, P.K. Madhu, S. Vega, High-resolution proton solid-state NMR spectroscopy by phase-modulated Lee-Goldburg experiment, Chem. Phys. Lett. 314 (1999) 443.
[5] E. Vinogradov, P.K. Madhu, S. Vega, A bimodal Floquet analysis of phase modulated Lee-Goldburg high resolution proton magic angle spinning NMR experiments, Chem. Phys. Lett. 329 (2000) 207.
[6] E. Vinogradov, P.K. Madhu, S. Vega, Phase modulated Lee-Goldburg magic angle spinning proton nuclear magnetic resonance experiments in the solid state: a bimodal Floquet theoretical treatment, J. Chem. Phys. 115 (2001) 8983.
[7] D. Sakellariou, A. Lesage, P. Hodgkinson, L. Emsley, Homonuclear dipolar decoupling in solid-state NMR using continuous phase modulation, Chem. Phys. Lett. 319 (2000) 253.
[8] P. Avenier, A. Lesage, M. Taoufik, A. Baudouin, A. De Mallmann, S. Fiddy, M. Vautier, L. Veyre, J.M. Basset, L. Emsley, E.A. Quadrelli, Well-defined surface imido amido tantalum(V) species from ammonia and silica-supported tantalum hydrides, J. Am. Chem. Soc. 129 (2007) 176.
[9] M. Leskes, S. Vega, Design of a triple quantum coherence excitation scheme for protons in solid state NMR, J. Chem. Phys. 130 (2009) 124506.
[10] E. Vinogradov, P.K. Madhu, S. Vega, Strategies for high-resolution proton spectroscopy in solid-state NMR, Topics Curr. Chem. 246 (2005) 33.
[11] S.P. Brown, Probing proton–proton proximities in the solid state, Prog. Nucl. Magn. Reson. Spectrosc. 50 (2007) 199.
[12] P.K. Madhu, High-resolution solid-state NMR spectroscopy of protons with homonuclear decoupling schemes under magic-angle spinning, Solid State Nucl. Magn. Reson. 35 (2009) 2–11.
[13] C. Coelho, J. Rocha, P.K. Madhu, L. Mafra, Practical aspects of Lee-Goldburg based CRAMPS techniques for high-resolution ^1H NMR spectroscopy in solids, J. Magn. Reson. 194 (2008) 264.
[14] L. Bosman, P.K. Madhu, E. Vinogradov, S. Vega, Improvement of homonuclear dipolar decoupling sequences in solid-state nuclear magnetic resonance utilising radiofrequency imperfections, J. Magn. Reson. 169 (2004) 39.
[15] M. Leskes, P.K. Madhu, S. Vega, Proton line narrowing in solid-state nuclear magnetic resonance: new insights from windowed phase-modulated Lee-Goldburg sequence, J. Chem. Phys. 125 (2006) 124506.
[16] M. Leskes, P.K. Madhu, S. Vega, A broad-banded z-rotation windowed phase-modulated LeeGoldburg pulse sequence for ^1H spectroscopy in solid-state NMR, Chem. Phys. Lett. 447 (2007) 370.
[17] E. Vinogradov, P.K. Madhu, S. Vega, Proton spectroscopy in solid state nuclear magnetic resonance with windowed phase-modulated Lee-Goldburg decoupling sequences, Chem. Phys. Lett. 354 (2002) 193.
[18] M. Leskes, P.K. Madhu, S. Vega, Supercycled homonuclear dipolar decoupling in solid-state NMR: toward cleaner ^1H spectrum and higher spinning rates, J. Chem. Phys. 128 (2008) 052309.
[19] M. Leskes, S. Steuernagel, D. Schneider, P.K. Madhu, S. Vega, Homonuclear dipolar decoupling at magic-angle spinning frequencies up to 65 kHz in solid-state nuclear magnetic resonance, Chem. Phys. Lett. 466 (2008) 95.
[20] S. Paul, R.S. Thakur, M. Goswami, A.C. Sauerwein, S. Mamone, M. Concistrè, H. Förster, M.H. Levitt, P.K. Madhu, Supercycled homonuclear dipolar decoupling sequences in solid-state NMR, J. Magn. Reson. 197 (2009) 14.
[21] D. Demco, S. Hafner, H.W. Spiess, Rotation-synchronized homonuclear dipolar decoupling, J. Magn. Reson. A 116 (1995) 36.
[22] S. Hafner, H.W. Spiess, Multiple-pulse line narrowing under fast magic-angle spinning, J. Magn. Reson. A 121 (1996) 160.
[23] P.K. Madhu, X. Zhao, M.H. Levitt, High-resolution ^1H NMR in the solid state using symmetry-based pulse sequences, Chem. Phys. Lett. 346 (2001) 142.
[24] S. Paul, R.S. Thakur, P.K. Madhu, ^1H homonuclear dipolar decoupling at high magic-angle spinning frequencies with rotor-synchronised symmetry sequences, Chem. Phys. Lett. 456 (2008) 253.
[25] J.P. Amoureux, B.Hu.J. Trebosc, Enhanced resolution in proton solid-state NMR with very-fast MAS experiments, J. Magn. Reson. 193 (2008) 305.
[26] J.P. Amoureux, B.Hu.J. Trebosc, F. Deng, Homonuclear dipolar decoupling schemes for fast MAS, Solid State Nucl. Magn. Reson. 35 (2009) 19.
[27] M.H. Levitt, Symmetry-based pulse sequences in magic-angle spinning solid-state NMR, in: D.M. Grant, R.K. Harris (Eds.), Encyclopedia of NMR, John Wiley & Sons, Chichester, 2002.
[28] D. Hoult, F.E. Richards, Critical factors in the design of sensitive high resolution nuclear magnetic resonance spectrometers, Proc. Roy. Soc. London A 334 (1975) 311.
[29] D. Marion, K. Wüthrich, Application of phase sensitive two-dimensional correlated spectroscopy (COSY) for measurements of ^1H–^1H spin-spin coupling constants in proteins, Biochem. Biophys. Res. Commun. 113 (1993) 967.
[30] M.H. Levitt, The sign of frequency and phases in NMR, J. Magn. Reson. 126 (1997) 164.
[31] E. Salager, R.S. Stein, S. Steuernagl, A. Lesage, B. Elena, L. Emsley, Enhanced sensitivity in high-resolution 1H solid-state NMR spectroscopy with DUMBO dipolar decoupling under ultra-fast MAS, Chem. Phys. Lett. 46 (2009) 336.
[32] G. Metz, X. Wu, S.O. Smith, Ramped-amplitude cross polarization in magic-angle-spinning NMR, J. Magn. Reson. A 110 (1994) 219.
[33] R.S. Thakur, N.D. Kurur, P.K. Madhu, Swept-frequency two-pulse phase modulation for heteronuclear dipolar decoupling in solid-state NMR, Chem. Phys. Lett. 426 (2006) 459.